ACS Catalysis

Research Article

pubs.acs.org/acscatalysis

# Effect of Enhanced Accessibility of Acid Sites in Micromesoporous Mordenite Zeolites on Hydroisomerization of *n*-Hexane

Jana Pastvova,[†,‡] Dalibor Kaucky,[†] Jaroslava Moravkova,[†] Jiri Rathousky,[†] Stepan Sklenak,[†] Maryna Vorokhta,[§] Libor Brabec,[†] Radim Pilar,[†] Ivo Jakubec,[∥] Edyta Tabor,[†] Petr Klein,[†] and Petr Sazama*[,†]

[†]J. Heyrovský Institute of Physical Chemistry, Academy of Sciences of the Czech Republic, Dolejskova 3, 182 23 Prague, Czech Republic

[‡]University of Pardubice, Studentská 95, 532 10 Pardubice, Czech Republic

[§]The Institute of Rock Structure and Mechanics, Academy of Sciences of the Czech Republic, V Holesovickach 94/41, 182 09 Prague, Czech Republic

[∥]Institute of Inorganic Chemistry, Academy of Sciences of the Czech Republic, Husinec-Rez, 25068 Rez, Czech Republic

Supporting Information

**ABSTRACT:** This paper describes a study of the nature and the accessibility of the acid sites in micromesoporous mordenite zeolites obtained by desilication and dealumination and analysis of their activity and selectivity in the hydroisomerization of *n*-hexane. Alkaline−acid, acid−alkaline−acid, and fluorination−alkaline−acid postsynthesis treatments were employed for the preparation of micromesoporous mordenites. The FTIR spectra of adsorbed $d_3$-acetonitrille, $^{27}$Al MAS NMR, HR-TEM, and $N_2$ adsorption were used for quantitative analysis of the Brønsted and Lewis sites, the coordination of Al atoms, and the textural properties. The alkaline treatment causes desilication, preferably occurring along the crystal defects and resulting in the formation of a secondary mesoporous structure characterized by 5−20 nm cavities and the formation of extraframework ($Al_{Ex}$) species and terminal Si−OH groups. The $Al_{Ex}$ species formed by hydrolysis of perturbed or dislodged framework Al easily restrict part of the pseudomonodimensional channel structure of mordenite. The subsequent removal of $Al_{Ex}$ by mild acid leaching or simultaneous removal of Si and Al atoms by desilication of fluorinated zeolite result in a micromesoporous structure with a large number of unrestricted channel openings and lead to a large increase in the accessibility of OH groups for *n*-hexane. Thus, the sequential leaching treatments enable the formation of active acid sites in an environment of nonrestricted microporous channels with simultaneous enhancement of accessibility of the active sites and molecular transport. It is shown that the micromesoporous structure with high concentration of Brønsted sites of enhanced accessibility directs the hydroisomerization reaction toward high yields of branched isomers and shortening of the main 12-ring channels and that the larger numbers of channel openings result in an increase in selectivity, limiting nonselective subsequent cracking reactions.

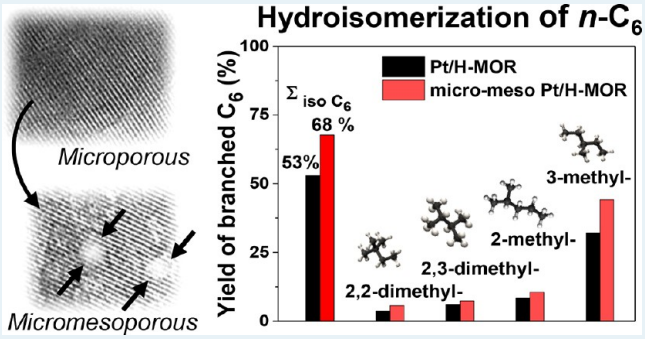


**KEYWORDS:** *isomerization, n-hexane, micromesoporous mordenite (MOR) zeolites, hierarchical structure, desilication*

## 1. INTRODUCTION

The isomerization of linear or low-branched alkane hydrocarbons via an intermediate alkene is an important process in oil refining for production of automotive fuels. The hydroisomerization of *n*-hexane transforms the linear isomer with low octane number into branched hexanes with sufficiently high octane numbers: e.g., the research octane numbers are 26 and 93 for *n*-hexane and 2,2-dimethylbutane, respectively. The process is typically catalyzed by bifunctional Pt/H-mordenite catalysts, and its complex mechanism consists of dehydrogenation of hexane to a hexene molecule on metallic platinum, skeletal isomerization of the hexene molecule on an acidic Brønsted site, and rehydrogenation of the branched hexene to hexane.[1−4] The acid-catalyzed reaction steps determine the overall reaction rate, while the dehydrogenation/hydrogenation reactions are usually in thermodynamic equilibrium and practically do not affect the reaction rate of the hydroisomerization.[4,5] Acid sites are located in mordenite zeolites in the small side pockets with eight-membered-ring (8-ring) openings and the main large straight channels with 12-ring openings (Figure 1) forming different local reaction environments affecting the confinement of a reactant molecule and

Received: May 24, 2017
Revised: July 17, 2017
Published: July 19, 2017

  

DOI: 10.1021/acscatal.7b01696
ACS Catal. 2017, 7, 5781−5795

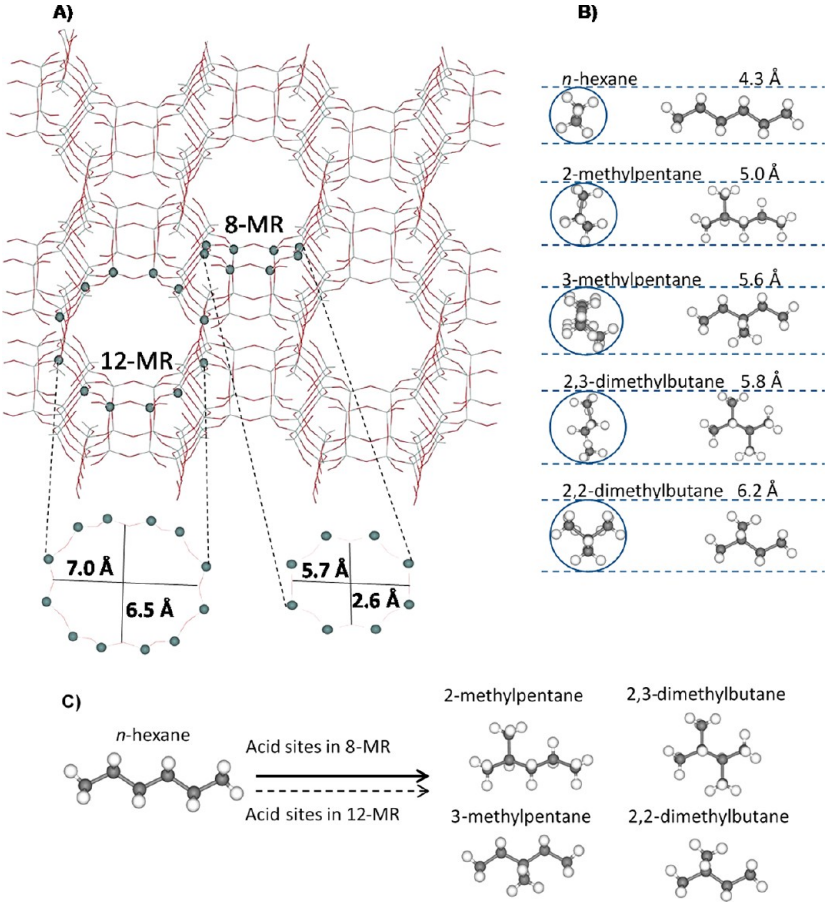


**Figure 1.** Illustration of the size-restriction of 8-ring in comparison to 12-ring channels in skeletal isomerization of *n*-hexane over mordenite zeolite: (A) topology of microporous mordenite zeolite consisting 12-ring (7.0 Å × 6.5 Å) channel and 8-ring (5.7 Å × 2.6 Å) side pockets; B) kinetic diameters of hexane isomers;[12] (C) reaction scheme.

corresponding adsorption enthalpy and stabilization of transition states.[6,7] The reaction rate of hydroisomerization of *n*-hexane over mordenites is thus controlled by the concentration of acid sites located in the 8-ring channel pockets and in the 12-ring main channels with 5 times higher turnover frequency (TOF) per proton in 8-ring channel pockets in comparison with that in 12-ring channels.[8]

Nevertheless, the accessibility of 8-ring (2.6 Å × 5.7 Å) in comparison to 12-ring (6.5 Å × 7.0 Å) channels is diffusion-restricted for *n*-hexane (cf. the size of the channel openings and kinetic diameters of the hexane isomers in Figure 1[9−12]) and the efficiency of the catalytic process is limited by mass transfer effects.[5,13] Because of their larger kinetic diameter, the branched hexanes diffuse even more slowly than *n*-hexane.[14] The accessibility of acid sites in the current industrial catalysts is enhanced by acid-treated partially dealuminated mordenites with improved textural properties.[5] However, dealumination leads to a decrease in the concentration of Brønsted sites, the formation of Lewis sites, and small changes in the micropores.[5] In recent years, considerable efforts have been devoted to improving the pore accessibility and molecular transport of reactants to active sites in micropores, namely in MFI zeolites, to enhance the activity in yielding the desired products in a variety of important acid-catalyzed reactions.[15−20] Several approaches have been developed to shorten the length of micropores and thus enhance mass transport by using zeolite nanosheets and nanocrystals[17,21,22] or zeolites that contain both micro- and mesopores. Micromesoporous (hierarchical) zeolites can be prepared by a variety of synthesis or postsynthesis methods, e.g., by confined crystal growth,[15,23] using polymers as mesoporogens,[13] or through postsynthesis desilication or dealumination processes.[11,18,24−26]

In the present work, we attempted to enhance the accessibility of the active sites by introducing secondary mesoporosity into mordenite zeolites coupled while attempting to preserve a large number of acid sites. The methods for effective formation of secondary mesoporosity through postsynthesis alkaline, alkaline−acid, acid−alkaline−acid, and fluorination−alkaline leaching procedures of conventional mordenite zeolites were explored in the preparation of micromesoporous zeolites with high concentrations of readily accessible Brønsted acid sites. In contrast to dealumination, controlled alkaline-based treatments of the mordenite framework lead to better preservation of the concentration of Brønsted sites and formation of well-developed secondary mesoporosity. The process was followed with respect to the state of Al and the concentration and accessibility of Brønsted sites and Al Lewis sites together with changes in the micromeso texture and how these parameters are reflected in *n*-hexane hydroisomerization over H/Pt-MOR.

## 2. EXPERIMENTAL SECTION

**2.1. Preparation of Micromesoporous H- and Pt/H-Mordenite Zeolites.** Mordenite zeolite (Zeolyst Int., CBV 20A molar Si/Al 12.1), denoted as MOR/12, was used for the



DOI: 10.1021/acscatal.7b01696
ACS Catal. 2017, 7, 5781−5795

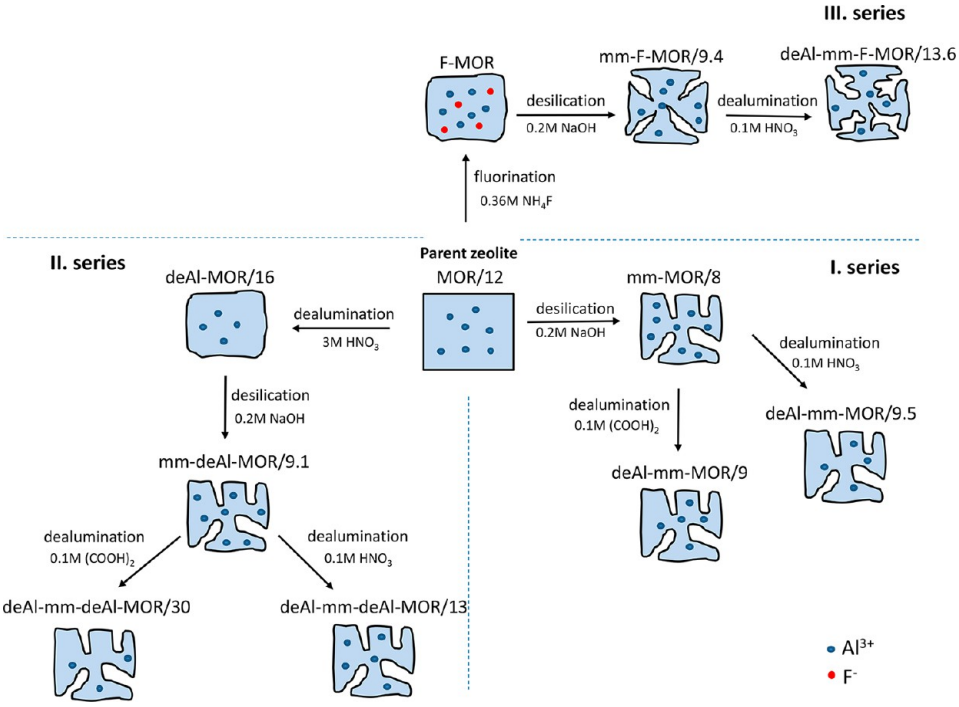


**Figure 2.** Scheme of the preparation of micromesoporous mordenite zeolites using postsynthesis alkaline−acid (series I), acid−alkaline−acid (series II), and fluorination−alkaline−acid (series III) leaching procedures.

preparation of micromesoporous mordenites using postsynthesis alkaline, alkaline−acid, acid−alkaline−acid, and fluorination−alkaline−acid leaching procedures (Figure 2) and as a standard for comparing catalytic properties. The first series of micromesoporous mordenites was prepared using alkaline and alkaline−acid treatments by leaching MOR/12 in an alkaline solution (30 mL of 0.2 M NaOH per 1 g of mordenite stirred in a beaker at 85 °C for 2 h, sample mm-MOR/8)[27] and subsequent leaching in acid solutions (30 mL of 0.1 M oxalic acid per 1 g of alkaline-treated zeolite stirred in a beaker at 85 °C for 20 h, sample deAl-mm-MOR/9, or 40 mL of 0.1 M $HNO_3$ per 1 g of alkaline-treated zeolite stirred in a beaker at 50 °C for 15 min, sample deAl-mm-MOR/9.5). The second series was prepared using acid−alkaline−acid treatments with dealumination of MOR/12 (30 mL of 3 M $HNO_3$ per 1 g of mordenite stirred and heated under reflux at 80 °C for 40 min, sample deAl-MOR/16), subsequent desilication (30 mL of 0.2 M NaOH per 1 g of dealuminated zeolite stirred in a beaker at 85 °C for 2 h, sample mm-deAl-MOR/9.1), and finally mild dealumination (30 mL of 0.1 M $HNO_3$ per 1 g of zeolite at 50 °C for 15 min, sample deAl-mm-deAl-MOR/13, or 30 mL of 0.1 M $(COOH)_2$ per 1 g of zeolite at 85 °C for 20 h, sample deAl-mm-deAl-MOR/30). The third series was prepared by fluorination of MOR/12 (5 g of mordenite was impregnated by 15 mL 0.36 M $NH_4F$ at room temperature, stored at room temperature for 8 h, and subsequently dried at 120 °C for 12 h), subsequent desilication (30 mL of 0.2 M NaOH per 1 g of fluorinated mordenite stirred in a beaker at 85 °C for 30 min) and calcination at 550 °C for 3 h (sample mm-F-MOR/9.4), with subsequent leaching in acid solutions (30 mL of 0.1 M $HNO_3$ per 1 g of zeolite at 50 °C for 15 min, sample deAl-mm-F-MOR-F/13.6).

All of the zeolites were ion-exchanged with 0.5 mol $dm^{-3}$ $NH_4NO_3$ at room temperature (1 g of a zeolite per 100 $cm^3$ of solution, three times over 12 h). Pt was introduced into the zeolites by incipient wetness impregnation with a $H_2PtCl_6$ solution to yield 1.5 wt % of Pt. The Pt-impregnated granulated zeolite was activated before the catalytic test in a stream of $O_2$ at 450 °C for 3 h, purged by a $N_2$ stream at 450 °C, followed by cooling to 250 °C, and finally activated in a mixture of 80 mol % of $H_2$ and 20 mol % of $N_2$ at 250 °C for 1 h.

**2.2. Characterization of Zeolites.** A Bruker AXSD8 Advance diffractometer with Cu K$\alpha$ radiation in Bragg−Brentano geometry with a graphite monochromator and a position-sensitive detector (Vântec-1) was used to record the X-ray powder diffraction (XRD) patterns. The porosity of the modified mordenites was determined by analysis of the adsorption isotherms of nitrogen at the boiling point of liquid nitrogen (77 K). Before the adsorption experiment, the samples were outgassed at 240 °C for at least 24 h to ensure complete cleaning of the surface. The experiments were carried out using an ASAP 2010 apparatus (Micromeritics). The volume of micropores and the external surface area were determined by the Broekhoff−de Boer *t* plot. The total pore volume was determined by converting the adsorption at the relative pressure of 0.8 to the volume of liquid nitrogen. The relative pressure around 0.8 for practically all of the investigated samples is high enough for complete filling of the pores and low enough to have substantial proportion in the interstitial space. The volume of mesopores was finally calculated by subtracting the volume of micropores from the total pore volume (at the relative pressure of 0.8). The crystal morphology was analyzed using a JEOL JSM-5500LV scanning electron microscope (SEM), (Figure S1 in the Supporting Information). High-resolution transmission electron microscopy (HR-TEM) was carried out on a JEOL JEM 3010 microscope operated at 300 kV ($LaB_6$ cathode, point resolution 1.7 Å). The length of the diffusion path in the mordenite channel in the crystal with the mesopores was estimated using a model approach as follows: the crystal size is 80 × 80 × 80 nm, and the volume



DOI: 10.1021/acscatal.7b01696
ACS Catal. 2017, 7, 5781−5795

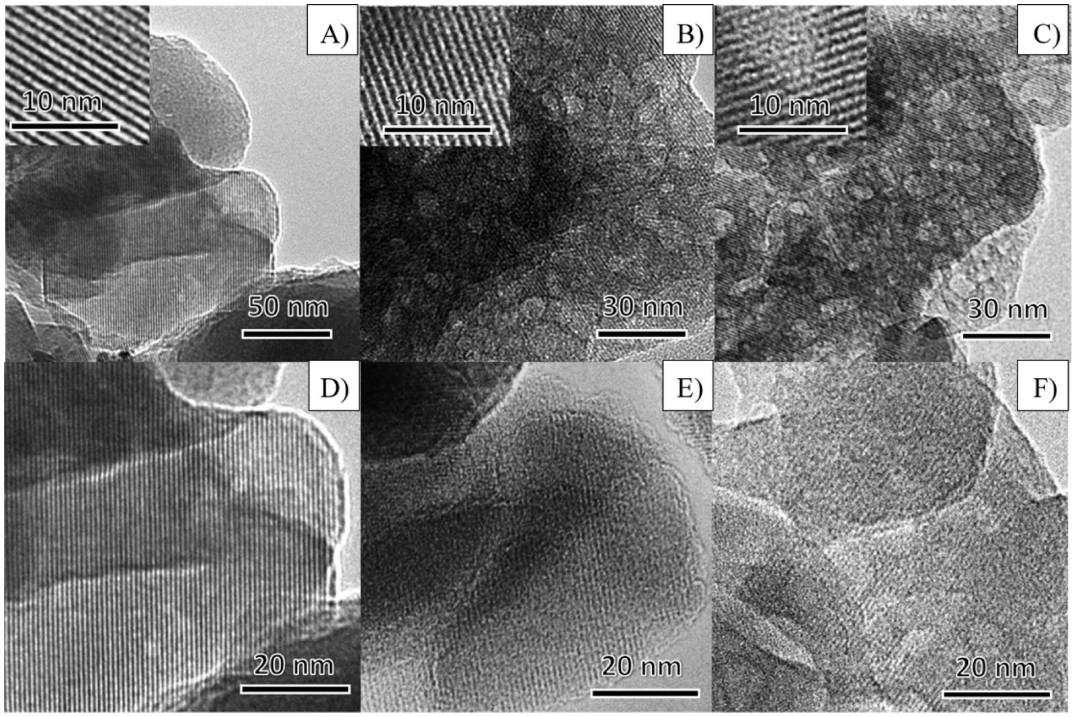


**Figure 3.** Representative HR-TEM images of (A, D) microporous MOR (MOR/12), (B) micromesoporous MOR (mm-MOR/8), (C) dealuminated micromesoporous (deAl-mm-MOR/9.5), (E) fluorinated MOR (F-MOR), and (F) fluorinated micromesoporous MOR (mm-F-MOR/9.4).

corresponding to the mesopores is 0.09 $cm^3\ g^{-1}$. Two cases were modeled: either 18 mesopores of 8 nm diameter or 72 mesopores of 4 nm diameter. The mesopores of length 80 nm were randomly positioned and oriented along one of the crystal axes. Three cases of diffusion paths were considered: the mordenite channel connects (i) one mesopore with the external surface of the crystal, (ii) two mesopores, and (iii) two external surfaces. One million simulations were used employing a pseudorandom number generator. The chemical compositions of the parent and prepared Pt-zeolites were determined by X-ray fluorescence spectroscopy using a PW 1404 instrument (Philips). The FTIR spectra of the zeolites evacuated at 450 °C for 3 h were recorded at room temperature on a Nicolet Nexus 670 FTIR spectrometer operating at 2 $cm^{-1}$ resolution by collecting 256 scans for a single spectrum. The adsorption of $d_3$-acetonitrile (13 mbar of $CD_3CN$ at room temperature for 20 min with subsequent evacuation for 15 min at room temperature) was used for analysis of the H-mordenites. The characteristic IR bands of the C≡N vibrations and the extinction coefficients $\varepsilon_B$ = 2.05 cm $\mu mol^{-1}$ and $\varepsilon_L$ = 3.60 cm $\mu mol^{-1}$ [28] were used for determination of the concentrations of acidic Brønsted and Lewis sites. The adsorption of *n*-hexane (1.4 Torr of *n*-hexane at room temperature for 20 min with gradual desorption to 0.005 Torr at room temperature) was used to estimate the accessibility of the OH groups of the mordenites for *n*-hexane. The difference between the intensity of the absorption bands of the OH groups in the spectra of the dehydrated mordenites and the spectra after adsorption of *n*-hexane provided information on the accessibility of the OH groups in mordenite. The desorption of *n*-hexane from the samples of microporous (MOR/12) and micromesoporous (deAl-mm-MOR/9.5) mordenites was followed by using a Nicolet 6700 FTIR spectrometer and an IR cell equipped with NaCl windows and connected to a vacuum line and *n*-hexane-dosing setup. The self-supported wafers with thickness <10 mg $cm^{-2}$ were evacuated prior the measurement at 450 °C for 3 h. The time-resolved in situ FTIR spectra were recorded at a resolution of 1 $cm^{-1}$ collected at a 0.2 s interval. The desorption of *n*-hexane was monitored after equilibration with *n*-hexane at a partial pressure 2.5 Torr at room temperature for 20 min and very fast decrease in the partial pressure from 2.5 to 1.5 Torr. Solid-state $^{27}Al$ and $^{29}Si$ MAS NMR experiments were carried out on a Bruker Avance 500 MHz Wide-Bore spectrometer (11.7 T) equipped with 4 mm double-resonance MAS NMR probe head. A high-power decoupling pulse sequence with a p/12 (0.7 $\mu s$) excitation pulse, 1 s relaxation delay, and rotation speed of 12 kHz was employed for measurement of the $^{27}Al$ MAS NMR spectra of fully hydrated samples. The chemical shifts were referenced to an aqueous solution of $Al(NO_3)_3$. $^{29}Si$ MAS NMR single-pulse spectra of hydrated zeolites were measured at a rotation speed of 7 kHz, with a $\pi/6$ (1.7 $\mu s$) excitation pulse and relaxation delay of 30 s for single-pulse spectra. The framework aluminum content ($Si/Al_{FR}$) was estimated from the intensity of the $^{29}Si$ NMR resonances according to the equation $Si/Al_{FR} = I/(0.25I_1 + 0.5I_2)$, where $I$, $I_1$, and $I_2$ correspond to the total, Si(3Si,1Al), and Si(2Si,2Al) intensities, respectively.[29,30]

**2.3. Catalytic Experiments.** The isomerization of *n*-hexane to the corresponding isohexanes was performed in a glass flow-through U-shaped reactor with spiral on the inlet part to enable preheating of the reactants, where the catalyst was supported inside the reactor on a porous-glass solid bed. Typically the reactor was filled with 0.5 g of the catalyst in the form of a grained solid (0.25−0.5 mm particle size fraction). The activation was performed before each catalytic test, and it consisted of two steps: first (i) the Pt-impregnated zeolite was activated by a stream of $O_2$ at 450 °C/3 h, briefly (0.25 h) purged by $N_2$ at 450 °C, and then the temperature was


DOI: 10.1021/acscatal.7b01696
ACS Catal. 2017, 7, 5781−5795

**Table 1. Preparation and Textural Properties of Micromesoporous Mordenite Zeolites**

| sample | preparation | Si/Al[a] | Si/Al$_{FR}$[b] | $V_{tot}$ ($P/P_0 \approx 0.8$) ($cm^3\ g^{-1}$) | $V_{MI}$[c] ($cm^3\ g^{-1}$) | $V_{MESO}$[d] ($cm^3\ g^{-1}$) | $S_{EXT}$[c] ($m^2\ g^{-1}$) |
|---|---|---|---|---|---|---|---|
| MOR/12 | microporous parent MOR | 12.1 | 12.5 | 0.24 | 0.19 | 0.05 | 42 |
| mm-MOR/8 | +0.2 M NaOH | 8.7 | 10.2 | 0.14 | 0.06 | 0.08 | 79 |
| deAl-mm-MOR/9 | +0.2 M NaOH + 0.1 M $(COOH)_2$ | 9 | 11.2 | 0.24 | 0.13 | 0.11 | 107 |
| deAl-mm-MOR/9.5 | +0.2 M NaOH +0.1 M $HNO_3$ | 9.5 | | 0.25 | 0.13 | 0.12 | 114 |
| deAl-MOR/16 | +3 M $HNO_3$ | 16.1 | | 0.24 | 0.19 | 0.05 | 44 |
| mm-deAl-MOR/9.1 | +3 M $HNO_3$ + 0.2 M NaOH | 9.1 | | 0.26 | 0.15 | 0.11 | 102 |
| deAl-mm-deAl-MOR/13 | +3 M $HNO_3$ + 0.2 M NaOH + 0.1 M $HNO_3$ | 13.5 | | 0.26 | 0.19 | 0.09 | 88 |
| deAl-mm-deAl-MOR/30 | +3 M $HNO_3$ + 0.2 M NaOH + 0.1 M $(COOH)_2$ | 30 | | 0.30 | 0.20 | 0.10 | 95 |
| mm-F-MOR/9.4 | +0.36 M $NH_4F$ + 0.2 M NaOH | 9.4 | | 0.23 | 0.14 | 0.09 | 104 |
| deAl-mm-F-MOR/13.6 | +0.36 M $NH_4F$ + 0.2 M NaOH + 0.1 M $HNO_3$ | 13.6 | | 0.22 | 0.14 | 0.08 | 104 |

[a]From chemical analysis. [b]From $^{29}$Si MAS NMR. [c]Estimated from the BdB *t* plot. [d]$V_{meso} = V_{total} - V_{micro}$.

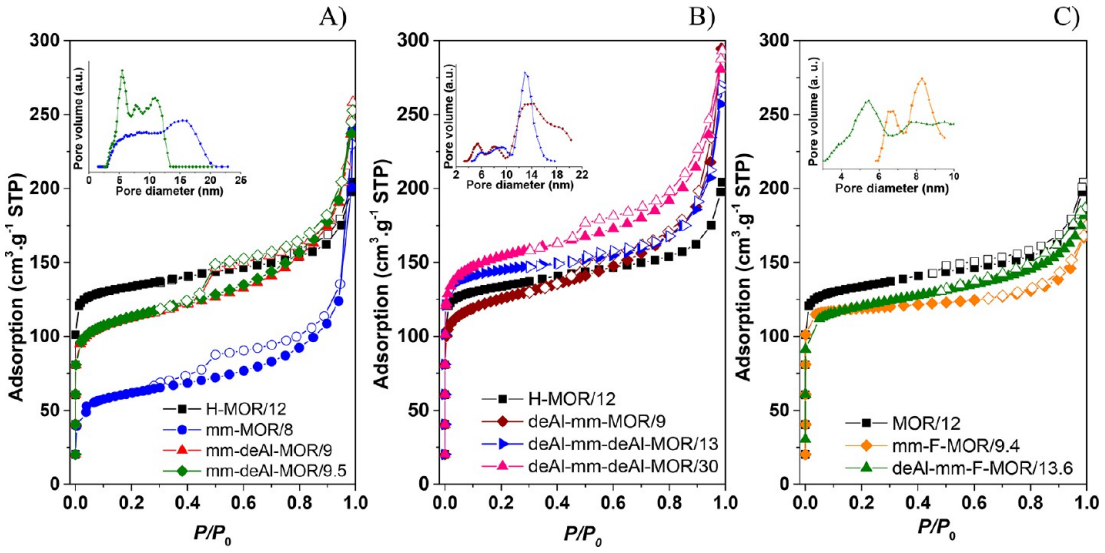


**Figure 4.** Nitrogen adsorption (solid symbols) and desorption (open symbols) at 77 K on microporous and micromesoporous mordenite zeolites prepared by sequential alkaline and acid leaching for (A) series I, (B) series II, and (C) series III.

**Table 2. Concentrations of Brønsted and Lewis Sites and the Accessibility of OH Groups in Micromesoporous Mordenites**

| | | $c$ (mmol $g^{-1}$) | | | | |
|---|---|---|---|---|---|---|
| sample | Si/Al[a] | $c_{Al}$[a] | $c_B$[b] | $c_L$[c] | $c_{B+2L}$[d] | accessibility of OH groups[e] (%) |
| MOR/12 | 12.1 | 1.23 | 1.06 | 0.12 | 1.30 | 64.1 |
| mm-MOR/8 | 8.7 | 1.49 | 0.44 | 0.14 | 0.72 | |
| deAl-mm-MOR/9 | 9 | 1.67 | 0.81 | 0.35 | 1.51 | 68.7 |
| deAl-mm-MOR/9.5 | 9.5 | 1.60 | 0.55 | 0.20 | 0.95 | 79.1 |
| deAl-MOR/16 | 16.1 | 0.97 | 0.47 | 0.13 | 0.73 | 92.6 |
| mm-deAl-MOR/9.1 | 9.1 | 1.65 | 0.44 | 0.22 | 0.88 | |
| deAl-mm-deAl-MOR/13 | 13.5 | 1.15 | 0.43 | 0.45 | 1.33 | 91.6 |
| deAl-mm-deAl-MOR/30 | 30 | 0.53 | 0.27 | 0.20 | 0.67 | 74.4 |
| mm-F-MOR/9.4 | 9.4 | 1.61 | 0.60 | 0.24 | 1.09 | 90.0 |

[a]From chemical analysis. [b]Concentrations of acid Brønsted sites from the FTIR spectra of adsorbed $d_3$-acetonitrile. [c]Concentrations of acid Lewis sites from the FTIR spectra of adsorbed $d_3$-acetonitrile. [d]Concentration of Al estimated from the concentration of Brønsted and Lewis sites ($c_{Al} = c_B + 2c_L$). [e]From the FTIR spectra of the bridging OH groups after adsorption of *n*-hexane.

decreased to 250 °C and second (ii) the sample was reduced at 250 °C by a mixture of 80% $H_2$ + 20% $N_2$ for 1 h. Then the *n*-hexane was cofed into the same feed of 79% $H_2$ + 20% $N_2$ by using a conventional saturator kept at the appropriate temperature. The total gas flow was thus adjusted to 66 $cm^3\ min^{-1}$, which corresponded to GHSV 5000 and WSHV 0.25 $h^{-1}$. The temperature in the reactor was measured with an immersed thermocouple and setup at the studied temperature in the 125−325 °C range. The composition of the outlet products, consisting of *n*-hexane, branched hexanes, and low molecular-weight products (i.e.: $C_1$, $C_2$, $C_3$, $C_4$, iso-$C_4$, $C_5$, and iso-$C_5$) was analyzed by an online sampling GC (Finnigan



DOI: 10.1021/acscatal.7b01696
ACS Catal. 2017, 7, 5781−5795

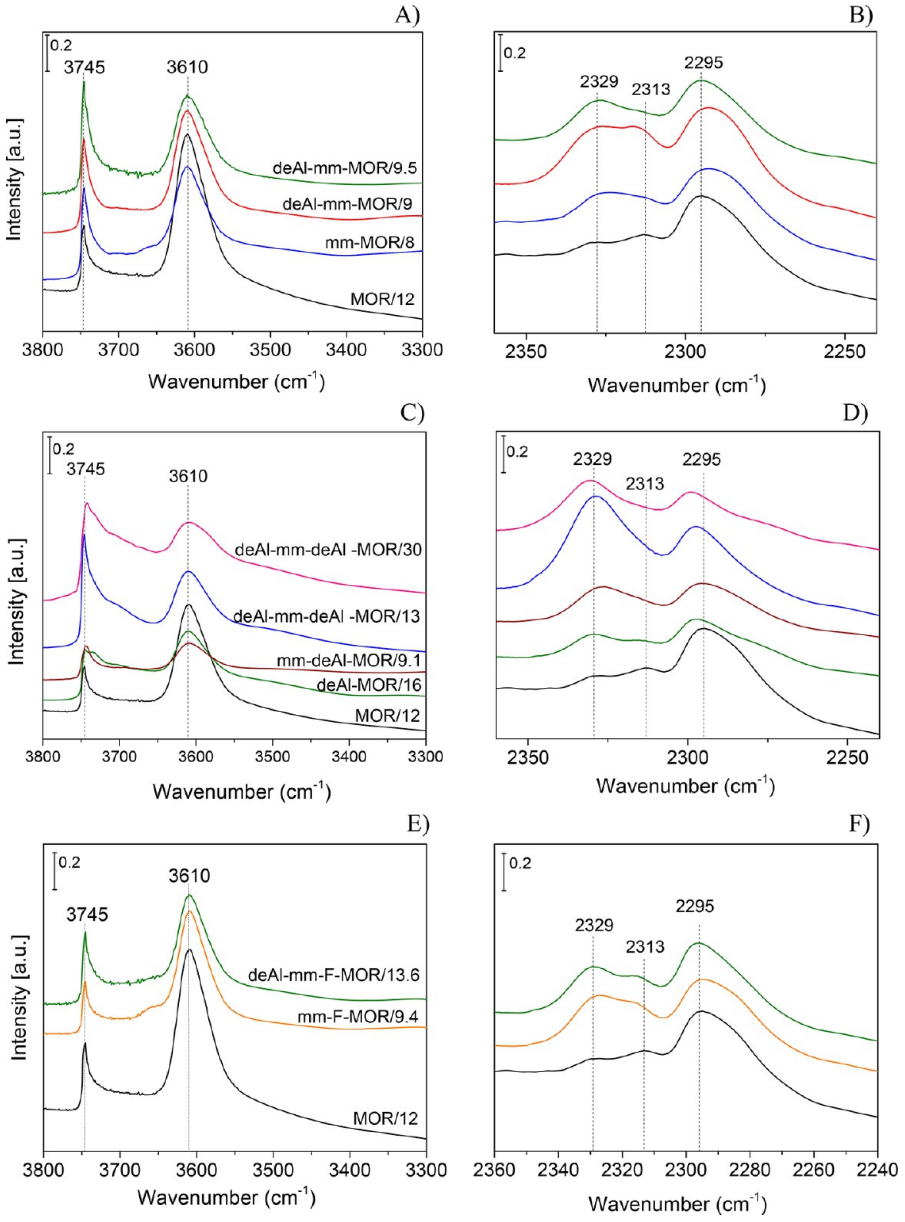


**Figure 5.** FTIR spectra of adsorbed $d_3$-acetonitrile (B, D, F) and FTIR spectra in the OH stretching region (A, C, and F) for microporous and micromesoporous H-MOR zeolites: (A, B) series I; (C, D) series II; (E, F) series III.

9001), equipped with a 50 m × 0.32 mm × 5 $\mu$m $Al_2O_3$/KCl column and detection enabled with a conventional FID detector. Steady-state conditions were usually achieved within 0.5−1 h of time on stream. The conversion and yield were expressed as

$$\text{conversion} = C_{0,n\text{-C6}} - C_{n\text{-C6}}/C_{0,n\text{-C6}} \times 10^2\ (\%)$$

$$\text{yield} = C_{\text{iso-C6}}/C_{0,n\text{-C6}} \times 10^2\ (\%)$$

where $C_{0,n\text{-C6}}$ was the concentration of *n*-hexane at the reactor inlet, while $C_{n\text{-C6}}$ and $C_{\text{iso-C6}}$ were the concentrations of *n*-hexane and of branched hexanes at the reactor outlet.

## 3. RESULTS

**3.1. Structural Analysis.** *3.1.1. Effect of Dealumination of Microporous Mordenite on the Concentration, Nature, and Accessibility of Acid Sites.* The microporous MOR/12 parent zeolite is characterized by a well-developed crystalline structure (Figure 3 and Figures S1 and S2 in the Supporting Information) with a microporous volume of 0.19 $cm^3\ g^{-1}$ (Table 1, Figure 4, and Figure S3 in the Supporting Information) and the presence of the majority of the Al in the framework in tetrahedral coordination (Figure S4 in the Supporting Information) (for details, see the Supporting Information). The FTIR spectra of the OH groups and adsorbed $d_3$-acetonitrile together indicate a slightly predominant concentration of Brønsted sites in the 12-ring in comparison to 8-ring channels, compensating the negative charge of regularly tetrahedrally coordinated Al in the framework, and a low concentration of Lewis acid sites (Table 2, Figure 5, and Figure S5 in the Supporting Information). Observation of the intensity of the infrared bands corresponding to OH groups in 8-ring and 12-ring channels upon introduction of *n*-hexane (Table 2 and Figure S6 in the Supporting Information) was used for estimation of the



DOI: 10.1021/acscatal.7b01696
ACS Catal. 2017, 7, 5781−5795

accessibility of OH groups located in the distinct channels. The band attributed to OH groups in the 8-ring channels of MOR was almost unperturbed after adsorption of *n*-hexane, indicating low accessibility of these OH groups for the probe molecule at room temperature. This is in accordance with the observation of very low accessibility of the acid sites located in 8-ring channels reported by Eder et al.[31] Both the experimental[32−34] and theoretical studies[35] of mordenite zeolites showed approximately one-third of the Brønsted hydroxyl groups heading toward the center of the 8-ring and the center of the side pocket, which is nonaccessible for larger molecules. This number seems to be independent of the Si/Al ratio[36] and is a result of the distribution of Al atoms in the four tetrahedral sites of mordenite;[32] this corresponds well to 64.1% of the accessible OH groups for *n*-hexane in H-MOR/12 (Table 2).

After partial dealumination of the framework of the parent mordenite zeolite by 3 M $HNO_3$, the Si/Al ratio was increased from 12 to 16 with a corresponding decrease in the concentration of the Brønsted sites, accompanied by an increase in the ratio of Lewis/Brønsted sites (Table 2) and a significant increase in the absorption bands at 3727 $cm^{-1}$, corresponding to internal silanol groups (Figure 5). The decrease in the concentration of the Brønsted sites and the increase in the band of internal silanol groups are consistent with the removal of the tetrahedrally coordinated framework Al atoms and the formation of four internal SiOH groups terminating the framework oxygen atoms. The structural changes induced by dealumination of mordenite zeolites have been described well in the scientific literature.[5,9,37] Removal of the framework Al atoms by acid leaching with nitric acid has been reported to result in secondary micropores that are larger than the main channels[5,37] or the formation of small mesopores,[5] improving the accessibility of the Brønsted OH groups remaining after dealumination in the side pockets. The similar adsorption/desorption branches of $N_2$ sorption without a hysteresis loop for both MOR/12 and deAl-MOR/16 indicate the absence of a significant volume in intracrystalline mesopores. The adsorption of *n*-hexane on deAl-MOR/16 caused a dramatic decrease in the intensity of the absorption bands of OH groups which clearly show that the Brønsted acid sites remaining in the deAl-MOR/16 sample zeolite after dealumination are readily accessible for the *n*-hexane molecule (>90%), (Table 2). The absence of mesopores, the increased accessibility of the OH groups, and the presence of internal silanol groups indicate that extraction of the framework Al atoms primarily induced changes in the distribution of the sizes and/or the connectivity of the microporous channels. However, in addition to appreciable textural changes, these structural changes caused a significant decrease in the concentration of the Brønsted acid sites to about half and an increase in the ratio of Lewis/Brønsted sites.

*3.1.2. Effect of Desilication on Structure of Mordenite.* TEM images of the alkaline-leached zeolite mm-MOR/8 (Figure 3) clearly show that the treatment resulted in extensive formation of a secondary mesoporous structure characterized by numerous cavities about 5−20 nm in size in the microporous crystals. The adsorption isotherms of desilicated mm-MOR/8 zeolite (Figure 4) exhibit a hysteresis loop typical for mesopores and adsorption in the zeolite micropores with a significant decrease in the volume of the micropores from 0.19 to 0.06 $cm^3\ g^{-1}$ (Table 1). The preservation of the crystalline structure of mm-MOR/8, which is obvious from the X-ray diffraction patterns (Figure S2 in the Supporting Information) and indirectly from the $^{29}Si$ MAS NMR spectrum (Table 1) and the lattice fringes in the HR-TEM images (Figure 3), indicates that the decrease in the microporous volume is not associated with collapse of the zeolitic structure but with blocking of the channel openings by $AlO_x$ extraframework plugs formed in the mesopores after desilication.[19] The extraframework Al species ($Al_{Ex}$) formed in the mesopores during desilication by hydrolysis of perturbed or dislodged framework Al enrich the surface[38] and can easily block a significant part of the pseudomonodimensional channel structure of mordenite.[19] The presence of $Al_{Ex}$ in mm-MOR/8 is obvious from (i) the broadening and decreasing of the symmetry of the signal at 55 ppm in the $^{27}Al$ MAS NMR spectra (Figure S4 in the Supporting Information) characteristic of variously perturbed Al species in the less-ordered environment in comparison to ideal tetrahedral coordination of Al atoms in the zeolite framework,[39−45] (ii) the additional spectral component around 3650−3670 $cm^{-1}$ (Figure 5) due to OH groups bound to extraframework and/or perturbed framework Al atoms,[46−48] (iii) a higher framework Si/Al ratio estimated from the $^{29}Si$ MAS NMR spectra in comparison to the value obtained from chemical analysis (Table 1), and (iv) a significant decrease in the concentration of Brønsted OH groups from 1.06 to 0.44 mmol $g^{-1}$ determined from the FTIR spectra of adsorbed $d_3$-acetonitrile.

Desilication of the partially dealuminated mordenite (deAl-MOR/16) resulted in a better developed secondary mesoporous structure in comparison to desilication of the parent mordenite, as indicated by higher and continuously increasing adsorption of $N_2$ at the relative pressures 0.1−0.8 and a hysteresis loop in the adsorption/desorption branches of the isotherm (Figure 4). After the alkaline treatments, the mesoporous volume increased to 0.08 and 0.11 $cm^3\ g^{-1}$ for mm-MOR/9 and mm-deAl-MOR/9.1, respectively (Table 1). It is well established that the presence of framework Al atoms stabilizes a neighboring siliceous part of the crystal and the extraction of Si is hindered for low Si/Al ratios.[25,49] Consequently, the lower content of Al in the framework of deAl-MOR/16 increased the susceptibility toward leaching of the framework Si atoms. Desilication is also preferred more along crystal defects,[50] which were densely created during the partial dealumination of the parent zeolite and which are reflected in the FTIR spectrum of deAl-MOR/16 in the absorption bands at 3727 $cm^{-1}$ of the internal silanol groups. The preferred desilication in the internal Si-related defects is manifested in a decrease in the intensity of the absorption at 3727 $cm^{-1}$ in the spectra of mm-deAl-MOR/9.1 in comparison to deAl-MOR/16. Thus, desilication is clearly enhanced upon prior partial dealumination of the microporous zeolite as a result of the higher susceptibility of the zeolite toward leaching at lower concentrations of framework Al atoms as well in the presence of the framework defect sites. The analysis of $N_2$-sorption isotherms by the Broekhoff−de Boer *t* plot shows a decrease in the micropore volume after desilication from 0.19 $cm^3\ g^{-1}$ in the parent zeolite to 0.06 and 0.15 $cm^3\ g^{-1}$ for mm-MOR/9 and mm-deAl-MOR/9.1, respectively (Table 1). It is probable that a lower concentration of Al in the parent zeolite and/or more developed mesoporosity providing a larger number of openings of the pseudomonodimensional channels lead to less blocking of the micropores in the mm-deAl-MOR/9.1 sample.

*3.1.3. Effect of Mild Acid Treatment on the Porous Structure and Accessibility of Acid Sites in Desilicated*



DOI: 10.1021/acscatal.7b01696
ACS Catal. 2017, 7, 5781−5795

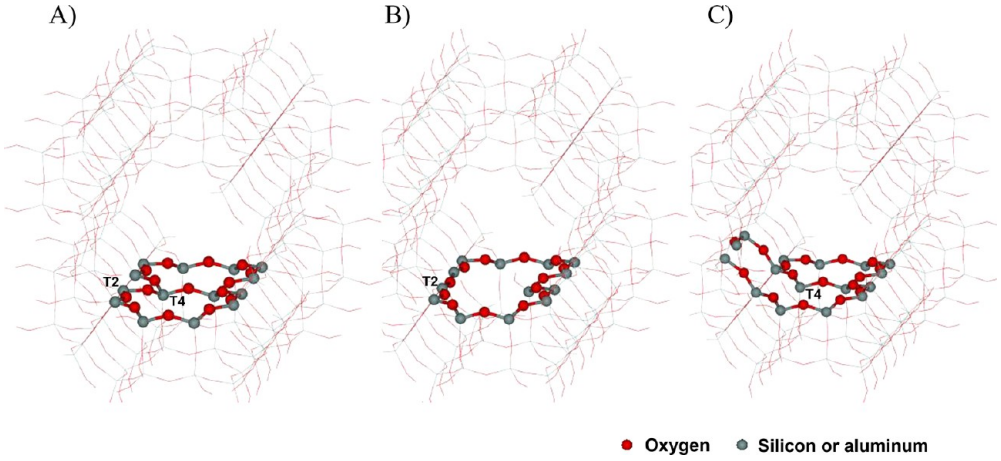


**Figure 6.** Schematic illustration of the effect of the extraction of one T atom from an 8-ring on the local structure of the openings of the side pockets in MOR zeolite: (A) two neighboring 8-rings and the same structure with removed (B) T4 atom and (C) T2 atom.

*Mordenite.* Our recent study[19] on the formation of secondary mesoporosity through postsynthesis sequential leaching procedures demonstrated that the Brønsted active sites located in the environment of nonrestricted micropores and accessible through mesopores can be obtained by alkaline and subsequent mild-acid leaching. Treatment of mm-MOR/8 using 0.1 M oxalic acid under mild conditions (deAl-mm-MOR/9) resulted in a very slight increase in the molar Si/Al ratio and a significant increase in the micropore volume from 0.06 to 0.13 $cm^3\ g^{-1}$ that further extended the volume of mesopores (Table 1), a significant increase in the concentration of Brønsted sites from 0.44 to 0.81 mmol $g^{-1}$ and Levis sites from 0.14 to 0.35 mmol $g^{-1}$ (Table 2), disappearance of the lowering symmetry of the signal at 55 ppm in the $^{27}Al$ MAS NMR spectra (Figure S4 in the Supporting Information), and elimination of the absorption band at 3650−3670 $cm^{-1}$ due to Al−OH groups (Figure 5). These findings clearly indicate that the extraframework and/or perturbed framework Al species formed in mesopores after desilication and blocking part of the micropores were removed by acid leaching. The increase in the concentrations of the acid sites indicates that the leaching selectively removed the extraframework tetrahedrally coordinated $AlO_x/(OH)_y$ species blocking the micropores, whereas the framework Al atoms associated with bridging OH groups were barely affected.

Acid leaching of mm-MOR/8 using 0.1 M nitric acid resulted in slightly more pronounced structural changes in comparison to the treatment using oxalic acid. Nitric acid, as a stronger dealumination agent,[51] caused a moderately greater increase in the molar Si/Al ratio, the same increase in the micropore volume from 0.06 to 0.13 $cm^3\ g^{-1}$, and further extension of the mesoporous volume to 0.12 $cm^3\ g^{-1}$ (Table 1). A lower concentration of Brønsted sites (0.55 mmol $g^{-1}$) indicates that part of the framework Al atoms was extracted from the framework and/or perturbed by the treatment in nitric acid. The removal of extraframework Al in the deAl-mm-MOR/9 sample by oxalic acid caused only minor changes in the availability of OH groups in comparison to the parent zeolite (Table 2). A significant increase in the accessibility of the OH groups (~80%) occurred after slight dealumination of the zeolite framework in the deAl-mm-MOR/9.5 sample by nitric acid. It seems that desilication with subsequent removal of extraframework Al can lead to shortening of the main 12-ring channels, but the number of new channel openings created in mesopores is not large enough for significant enhancement of the accessibility of the OH groups in 8-ring side pockets.

Partial dealumination of mm-deAl-MOR/9.1 using 0.1 M nitric acid caused similar changes to the dealumination of mm-MOR/8. However, they are less pronounced: i.e., opening of restricted micropores with an increase in the volume of micropores from 0.15 to 0.19 $cm^3\ g^1$ and increase in the concentration of Lewis sites from 0.22 to 0.45 mmol $g^{-1}$. The concentration (0.43 mmol $g^{-1}$) and accessibility of Brønsted acid sites (~92%) are very comparable with those of deAl-MOR/16. Thus, the desilication of deAl-MOR/16 with subsequent removal of $Al_{Ex}$ by mild acid leaching resulted in deAl-mm-deAl-MOR/13 with well-developed mesoporous structure and with similar concentration and accessibility of OH groups for *n*-hexane as the starting deAl-MOR/16 before the subsequent alkaline−acid treatments.

The hydrolysis of Al−O and Si−O bonds in the 8-ring (formed by T2 and T4 atoms) during acid and alkaline treatments results in dislodgement of the T atom from the framework position and dramatic changes in the local arrangement. Figure 6 illustrates how the openings of two neighboring side pockets in MOR zeolite can be altered by the removal of one T atom in the T2 or T4 sites. The extraction of the T4 atom leads to a merging of the two 8-rings, providing a large void space enabling a diffusion of large molecules: e.g., benzene.[52] The extraction of the T2 atom could possibly provide a large deformed elongated ring; however, previous reports indicate that the extraction is site specific and the dealumination of T4 is strongly favored.[52−54] The creation of these open connections by the preferable extraction of Al atoms from the T4 sites explains the dramatic increase in the accessibility of the bridging of OH for hexane even after very mild dealumination of the mordenite framework.

*3.1.4. Effect of Fluorination−Alkaline Treatment on the Porous Structure and Accessibility of Acid Sites in Mordenite.* Recently, Yu et al.[55] showed that impregnation of microporous ZSM-5 zeolite with an aqueous solution of $NH_4F$ prior leaching by a solution of NaOH increases the susceptibility of the zeolite toward leaching of framework Al atoms and provides controlled extraction of both Al and Si atoms. We modified the procedure for alkaline treatment of fluorinated mordenites and obtained the mordenite zeolite mm-F-MOR/9.4 with the mesopore volume increased to 0.09 $cm^3\ g^{-1}$ and the volume of the micropores concurrently slightly decreased to 0.14 $cm^3\ g^{-1}$,



DOI: 10.1021/acscatal.7b01696
ACS Catal. 2017, 7, 5781−5795

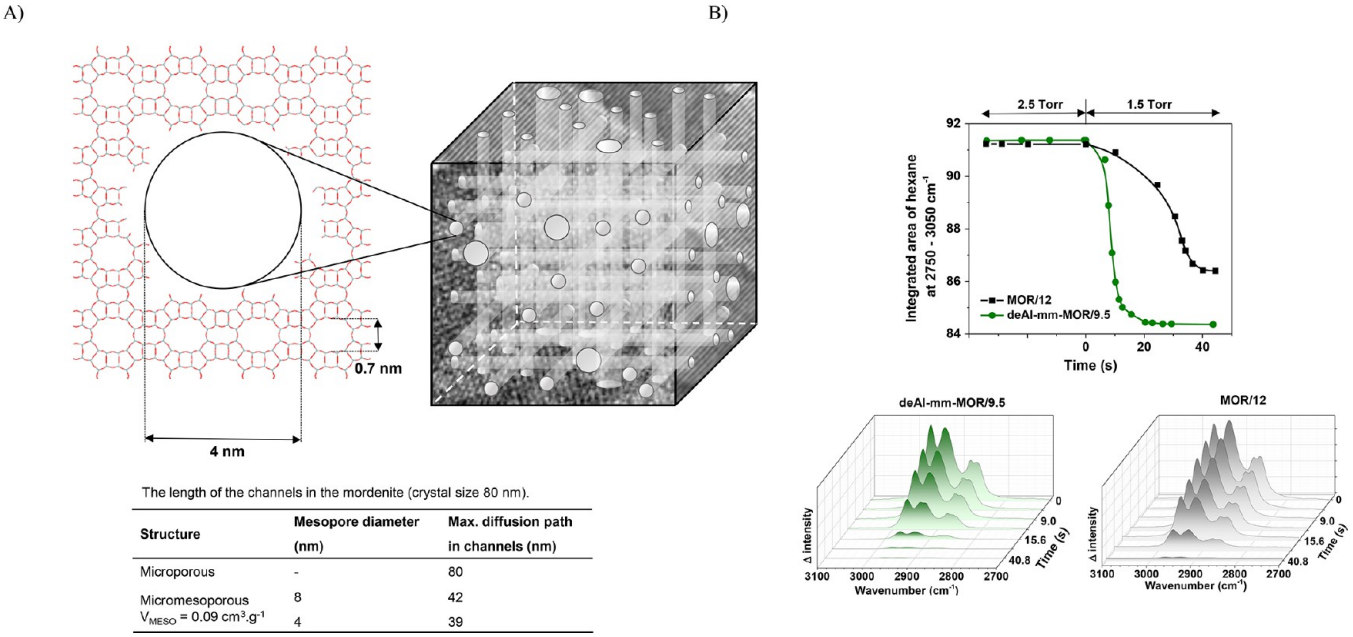


The length of the channels in the mordenite (crystal size 80 nm).

| Structure | Mesopore diameter (nm) | Max. diffusion path in channels (nm) |
|---|---|---|
| Microporous | - | 80 |
| Micromesoporous $V_{MESO}$ = 0.09 $cm^3.g^{-1}$ | 8 | 42 |
| | 4 | 39 |

**Figure 7.** Analysis of the effect of the presence of mesopores on the length of zeolite channels and diffusion of *n*-hexane: (A) model determining the length of the diffusion path through the mordenite channel, where 4 and 8 nm channels oriented along the axes and internal mesopore volume 0.09 $cm^3\ g^{-1}$ were considered; (B) desorption of *n*-hexane initiated by changes in the *n*-hexane partial pressure from 2.5 to 1.5 Torr analyzed by FTIR spectroscopy.

indicating the formation of secondary mesoporosity and opening of nonrestricted channel openings of the preserved microporous structure. In addition to the small, near-circular bright areas reflecting formation of intracrystalline mesoporosity, HR-TEM images (Figure 3) also show mesopores formed along boundaries and intergrowths. The dissolution or etching along boundaries and intergrowths and the indiscriminate dissolution of Al and Si are characteristic of chemical etching with fluoride ions in $NH_4F$-HF,[56] and Al-directed dissolution of siliceous areas is typical for alkaline treatment.[57] Two modes of the formation of the mesoporous structure were also reported by Svelle et al.[50] for standard desilication. They demonstrated the creation of mesopores as a consequence of both Al-directed dissolution of siliceous areas and selective dissolution or etching along boundaries, intergrowths, and defects within each particle. HR-TEM images of mm-F-MOR/9.4 show concomitant contribution of both modes of mesopore formation. The slight shift of the maximum of the peak at about 55 ppm in the $^{27}$Al MAS NMR spectra (Figure S4 in the Supporting Information) reflects changes in the coordination and local surroundings of the Al sites and/or a site-specific dealumination of the individual T sites.[52−54] The concentration of Brønsted and Lewis sites, 0.6 and 0.24 mmol $g^{-1}$, respectively, determined by adsorption of $d_3$-acetonitrile, and high accessibility (>90%) of bridging OH groups for *n*-hexane molecule (Table 2) for the mm-F-MOR/9.4 sample show that the desilication of fluorinated mordenite zeolite yields a micromesoporous structure with high concentration of readily accessible acid sites. The development of secondary mesoporosity and preservation of microporosity via concurrent extraction of $SiO_2$ and a smaller amount of Al is enabled by transformation of a fraction of Si−O−Al into the framework as F-bearing tetrahedral Al entities after fluorination.[55] The presence of F-bearing tetrahedral Al species which are readily dislodged in alkaline medium[55] and Al sites in Si−O−Al entities with persistent resistance to alkaline treatment enabled controlled Al and Si extraction during the alkaline treatment. The finding that this treatment significantly improved the accessibility of OH groups for *n*-hexane is of great importance. The simultaneous removal of Si and Al atoms and smaller size of part of the formed mesopores with possibly a larger number of new channel openings results in a large increase in the accessibility of the OH groups for *n*-hexane.

*3.1.5. Effect of Mesoporosity on the Pore Length.* In order to illustrate the effect of mesoporosity on the reactant transport, a model showing the shortening of the main 12-ring channels was made and the desorption of *n*-hexane was analyzed for the microporous and a representative micromesoporous mordenite (Figure 7). The model is based on the obtained SEM, HR-TEM, and $N_2$ adsorption data considering the mesoporous volume 0.09 $cm^3\ g^{-1}$, which is approximately 15% of the total volume of the crystal, and the crystal size of 80 nm. Two cases were modeled with randomly positioned mesopores of diameter 4 or 8 nm oriented along one of the crystal axes and connected to the external surface of the crystal. The mesopores that communicate with the external surface of the mordenite crystal are observed in the high-resolution TEM images, and the spatial arrangement of the mesopores in the entire void volume of the crystal was demonstrated by Milina et al.[58] using positron annihilation lifetime spectroscopy for micromesoporous zeolites prepared by desilication using the same amount and concentration of NaOH solution. Three cases of the diffusion paths were considered: the mordenite channel connects (i) one mesopore with the external surface of the crystal, (ii) two mesopores, and (iii) two external surfaces (i.e., the diffusion path 80 nm) if there is no mesopore present. One million simulations using a pseudorandom number generator yielded diffusion paths of 42 and 39 nm for the mesopores of the 8 and 4 nm diameters, respectively. The diffusion path depends only slightly on the diameter of the mesopores, since only approximately 15% of the crystal is


DOI: 10.1021/acscatal.7b01696
ACS Catal. 2017, 7, 5781−5795

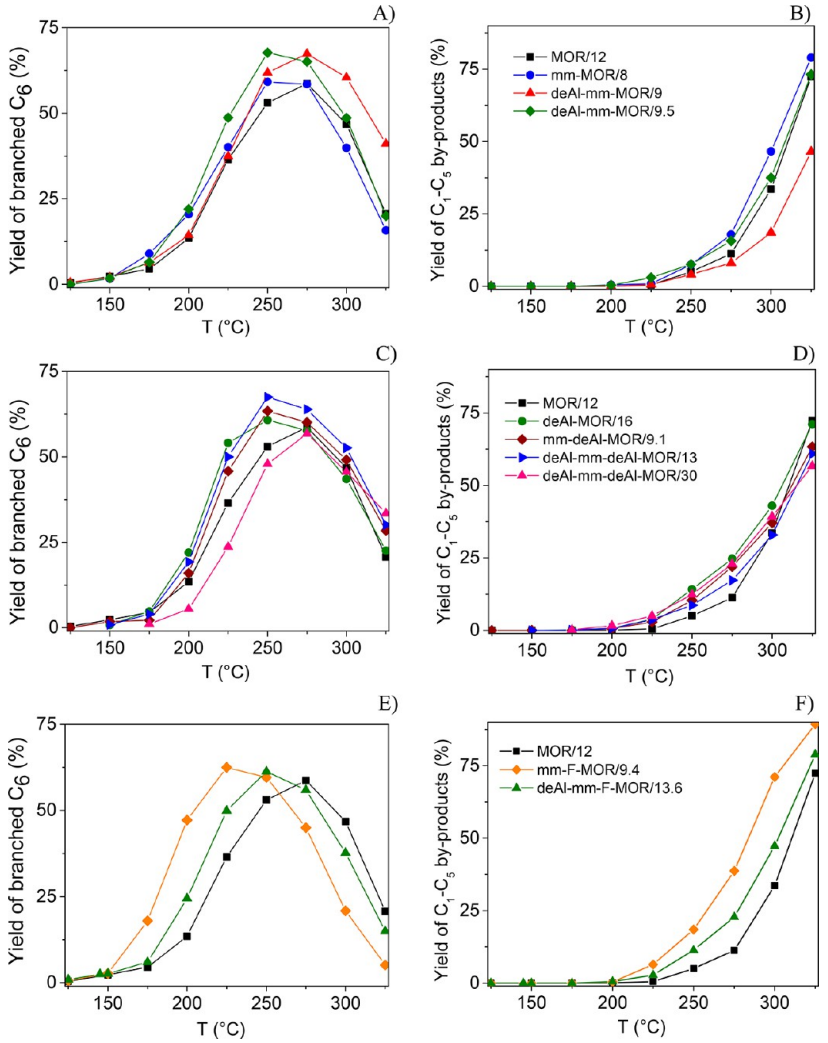


**Figure 8.** Yields of branched $C_6$ isomers and $C_1$−$C_5$ byproducts in the hydroisomerization of *n*-hexane over Pt/H-MOR zeolites as a function of temperature: (A, B) series I; (C, D) series II; (E, F) series III.

removed and a majority of the crystal is not influenced by the mesopores.

The series of FTIR spectra recorded during transient desorption of *n*-hexane induced by a very fast decrease in the partial pressure of *n*-hexane from 2.5 to 1.5 Torr are shown for MOR/12 and deAl-mm-MOR/9.5 in Figure 7B. The partial pressure of 1.5 Torr provides the loading of one *n*-hexane molecule per acid site, while *n*-hexane molecules weakly interacting with the inert channel walls are also present at the partial pressure of 2.5 Torr. Under such a decrease in the partial pressure, the changes in transport can be associated with the alterations of the pore structure rather than with desorption of *n*-hexane from the acid sites. The higher desorption rate observed for the micromesoporous deAl-mm-MOR/9.5 in comparison to microporous MOR/12 is thus consistent with the effective reduction of the crystal domain by the introduction of the mesopores communicating with both the micropores and connected with the external surface. The enhanced transport in the micromesoporous zeolite can also be, however, affected by a contribution from a complex interplay of changes in the local structure of microporous channels and the channel openings.[59]

*3.1.6. Structure of Pt Species.* Ribeiro et al.[60] showed that the reaction rate in the hydroisomerization reaction is practically independent of the surface of the metallic platinum clusters for platinum loadings from 0.5 to 6 wt % in Pt-faujasite zeolites. Consistently, Van de Runstraat et al.[61] showed that the hydrogenation/dehydrogenation functions of platinum was not rate-determining for Pt/H-*BEA with a platinum loading of ∼1.5 wt %. Accordingly, to ensure that the dehydrogenation/hydrogenation reactions do not limit the overall alkane hydroisomerization, all of the Pt/H-MOR catalysts were prepared with a concentration of 1.5 wt % Pt and the dispersity of the platinum clusters was checked using HR-TEM and FTIR spectra of adsorbed CO. Well-dispersed platinum clusters with particle sizes ∼1−20 nm located on the external surface of the zeolite crystals were observed in the HR-TEM images of all the microporous and micromesoporous Pt-MOR zeolites (Figure S7 in the Supporting Information). The broad distribution of the Pt cluster sizes is typical for Pt-zeolites prepared by conventional incipient wetness impregnation. Similar intensities of the absorption bands of the hydroxyl group in the FTIR spectra before and after impregnation of the mordenites with platinum indicate that the Pt reduced under a hydrogen atmosphere is not coordinated in cationic sites to a significant extent (not shown). The FTIR spectra of CO adsorbed on microporous and micromesoporous Pt/H-MOR zeolites (Figure S8 in the Supporting Information) exhibit the presence



DOI: 10.1021/acscatal.7b01696
ACS Catal. 2017, 7, 5781−5795

Table 3. Yields of Branched Hexane Isomers and Lower Molecular Weight Byproducts for Hydroisomerization of *n*-Hexane over Microporous and Micromesoporous Pt/H-MOR at 225 and 250 °C

| | $\sum y_{iso\text{-}C6}$ (%) | | 2,2-dimethyl (%) | | 2,3-dimethyl (%) | | 2-methyl (%) | | 3-methyl (%) | | $C_1-C_5$ (%) | |
|---|---|---|---|---|---|---|---|---|---|---|---|---|
| sample | 225 °C | 250 °C | 225 °C | 250 °C | 225 °C | 250 °C | 225 °C | 250 °C | 225 °C | 250 °C | 225 °C | 250 °C |
| Pt/H-MOR/12 | 36.5 | 53.0 | 1.6 | 3.6 | 6.0 | 6.0 | 7.3 | 8.4 | 21.6 | 35 | 0.5 | 5.3 |
| Pt/H-mm-MOR/8 | 40.1 | 59.2 | 2.5 | 5.2 | 5.2 | 6.3 | 7.9 | 8.6 | 24.5 | 39.1 | 0.9 | 7.5 |
| Pt/H-deAl-mm-MOR/9 | 37.5 | 61.9 | 2.1 | 5.4 | 4.7 | 6.7 | 8.7 | 8.7 | 22.0 | 41.1 | 0.6 | 4.1 |
| Pt/H-deAl-mm-MOR/9.5 | 48.7 | 67.7 | 1.8 | 5.7 | 6.1 | 7.3 | 8.8 | 10.5 | 32.0 | 44.2 | 3.0 | 7.6 |
| Pt/H-deAl-MOR/16 | 54.1 | 60.8 | 2.9 | 4.9 | 6.1 | 6.8 | 11.2 | 11.3 | 33.9 | 37.8 | 3.9 | 16 |
| Pt/H-mm-deAl-MOR/9.1 | 45.8 | 63.4 | 2.8 | 8.1 | 4.5 | 6.5 | 8.6 | 8.6 | 29.9 | 40.2 | 2.9 | 10.4 |
| Pt/H-deAl-mm-deAl-MOR/13 | 50.0 | 67.5 | 2.4 | 6.3 | 5.0 | 7.4 | 8.2 | 10.0 | 34.4 | 43.8 | 3.7 | 8.7 |
| Pt/H-deAl-mm-deAl-MOR/30 | 23.7 | 47.9 | 0.6 | 3.5 | 1.3 | 4.2 | 7.3 | 8.4 | 14.5 | 31.8 | 5.0 | 12.4 |
| Pt/H-mm-F-MOR/9.4 | 62.5 | 59.6 | 4.9 | 7.4 | 7.4 | 6.2 | 8.6 | 8.4 | 41.6 | 37.6 | 6.4 | 18.5 |

of a broad absorption band at 2078 $cm^{-1}$ characteristic for reduced Pt metallic clusters 1−20 nm in size[62,63] located on the external surface of the zeolite crystal. The reduction of Pt into the zerovalent oxidation state of metallic Pt is also indicated by the absence of the absorption bands at 2170−2150 $cm^{-1}$ and at 2130−2140 $cm^{-1}$ characteristic of CO interacting with $Pt^{2+}$ counterions and $Pt_n^{\delta+}$ clusters, respectively.[62,63] Thus, all of the Pt/H-MOR contains well-dispersed platinum in the form of metallic clusters that can provide sufficient hydrogenation/dehydrogenation reactions occurring for the employed Pt loadings much more rapidly than isomerization reactions on acid sites, regardless of the specifics of their structure for all of the Pt/H-zeolite catalysts.[60,64]

The presence of the secondary mesoporous structure can possibly increase the proximity between the metallic platinum and the Brønsted sites. The effect of nanoscale proximity of metallic sites and acid sites on the hydroconversion of hydrocarbons was recently assessed by Zecevic et al.[65] They showed that the closest proximity between the metal and the Brønsted acid sites in zeolites does not provide improved catalytic properties in hydrocracking reactions. This is in line with the results of our study on hydroisomerization,[66] where we analyzed whether the activity of Pt/H-MOR zeolite is affected by the proximity of Pt species and acid sites using the samples of H-MOR/12-Pt/$Al_2O_3$ prepared as mechanical mixtures of the protonic form of the zeolite and Pt/$Al_2O_3$. The yields were practically identical for both the Pt/H-MOR and H-MOR/12-Pt/$Al_2O_3$ with platinum metal deposited on either the zeolite or alumina.[66]

**3.2. Hydroisomerization of *n*-Hexane.** *3.2.1. Hydroisomerization over Microporous, Desilicated, and Partially Dealuminated-Desilicated Mordenites.* Figure 8 depicts the yields of branched hexane isomers (2-methylpentane, 3-methylpentane, 2,2-dimethylbutane, and 2,3-dimethylbutane) and $C_1-C_5$ byproducts (methane, ethane, propane, butanes, and pentanes) as a function of the reaction temperature in the hydroisomerization of *n*-hexane over the microporous and micromesoporous Pt/H-MOR zeolites. The yields of the individual products at 225 and 250 °C are given in Table 3. With microporous MOR/12, the conversion first started to increase at a temperature of approximately 150 °C and reached a maximum of 58% at approximately 275 °C before declining again due to nonselective cracking reactions, as is indicated by the steadily increasing conversion of *n*-hexane and yield of $C_1-C_5$ byproducts. The desilication of the parent sample resulted in little improvement in conversions over the entire temperature range, passing through a maximum at 250 °C with the yields increasing from 53.0 to 59.2% and from 9.6 to 11.5% for all of the branched and dibranched hexanes, respectively, and then declining due to nonselective cracking at higher temperatures. The catalytic behavior of the mm-MOR/8 sample is in accordance with the findings of Monteiro et al.,[67] showing that the desilication of mordenite zeolite does not significantly improve the catalytic efficiency of the mordenite zeolites.

With the deAl-mm-MOR/9 sample obtained by the removal of extraframework Al from mm-MOR/8 using oxalic acid, the formation of byproducts at high temperatures was significantly reduced in comparison to mm-MOR/8 or microporous MOR/12 samples and was accompanied by a corresponding increase in the yield of the desired branched isomers, reaching a maximum of 67.4% at 275 °C. The deAl-mm-MOR/9 sample is characterized by shortened 12-ring channels due to a well-developed secondary mesoporous structure, but without significantly enhanced accessibility of the OH groups in comparison to the parent zeolite (Table 2). It seems that the shortening of the main channel and a larger number of channel openings provide only a slight increase in activity but lead to a significant increase in selectivity, limiting the nonselective subsequent cracking reactions and consequently increasing the yield of desired products at higher temperatures.

The deAl-mm-MOR/9.5 sample dealuminated by nitric acid provides higher yields of branched isomers in comparison to MOR/12 and mm-MOR/8 zeolites with similar yields of byproducts (Figure 8). As the difference between deAl-mm-MOR/9.5 and deAl-mm-MOR/9 lies mainly in the significantly higher accessibility of the OH groups (Table 2), the improvements in the yields of branched isomers at lower temperatures, e.g. from 53% to 67.7% at 250 °C, can be associated with greater accessibility of the acid sites and the improvements in the yield at higher temperatures, e.g. from 58.7 to 67.4% at 275 °C, also with the shortened main channels and larger number of channel openings. Thus, the use of the deAl-mm-MOR/9.5 sample had a positive effect on the yield of branched isomers in the whole temperature region. The improvements in the catalytic properties are minor, however, clearly indicating the potential for improvements in the functionality of hydroisomerization mordenite catalysts via enhanced accessibility of active sites and transport of reactants in the micromesoporous structure.

The durability and stability of the catalytic activity for the deAl-mm-MOR/9.5 as a representative micromesoporous Pt/H-MOR zeolite were analyzed under the reaction conditions. Stable values of the yields of mono- and dibranched isomers, ∼55% and ∼9%, respectively, and byproducts ∼1% as a function of time on stream were obtained over deAl-mm-MOR/9.5 at 235 °C for 72 h, indicating a sufficient structural



DOI: 10.1021/acscatal.7b01696
ACS Catal. 2017, 7, 5781−5795

stability and no deactivation of the micromesoporous Pt/H-MOR (Figure 9).

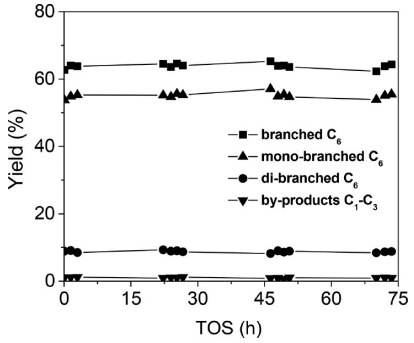


**Figure 9.** Dependence of the yield of branched hexane isomers and $C_1$−$C_3$ byproducts on time on stream (TOS) in hydroisomerization of *n*-hexane over Pt/H-deAl-mm-MOR/9.5 at 235 °C.

*3.2.2. Hydroisomerization over Partially Dealuminated and Acid−Alkaline−Acid-Treated Mordenites.* Figure 8C shows the yields of branched isomers as a function of temperature obtained over dealuminated deAl-MOR/16 and zeolites prepared by subsequent desilication and desilication/dealumination of the deAl-MOR/16 sample. Although the dealumination of mordenite (deAl-MOR/16) leads to a decrease in the concentration of Brønsted sites from 1.06 to 0.47 mmol $g^{-1}$, the accessibility of the remaining acid sites was significantly enhanced, with ∼92% of the Brønsted sites accessible for *n*-hexane (Table 2). Less than half the concentration of Brønsted sites in deAl-MOR/16 provided yields of branched hexanes which outperform the microporous MOR/12: see, for example, the yields of branched hexanes 36.5% and 54.1% at 225 °C for MOR/12 and deAl-MOR/16, respectively. The higher specific activity of acid-treated partially dealuminated mordenites has been well documented in the literature[68] and explained by the beneficial effects on the textural properties of extraction of part of the framework Al atoms by acid treatment, leading to improved accessibility of highly active acid sites located in the 8-ring side pockets.[5,69] Desilication of the deAl-MOR/16 sample yielded micro-mesoporous mm-deAl-MOR/9, which showed no significant changes in the yields of the branched isomers nor byproducts. The positive effect of the development of the mesoporous volume (0.11 $cm^3$ $g^{-1}$) was probably offset by the negative effect of the decline in the microporous volume because of its partial blockage. The subsequent partial dealumination of mm-deAl-MOR/9 provided the deAl-mm-deAl-MOR/13 sample with a well-developed mesoporous structure and with similar concentration and accessibility of the OH groups for *n*-hexane in comparison to the deAl-MOR/16 sample. The similar concentrations and accessibility of the OH groups for *n*-hexane in the deAl-MOR/16 and deAl-mm-deAl-MOR/13 samples resulted in similar yields of branched hexane isomers at ≤225 °C. The presence of mesoporous structures in deAl-mm-deAl-MOR/13 caused a slightly lower formation of cracking products and a corresponding increase in the yield of branched hexanes at temperatures ≥250 °C.

*3.2.3. Hydroisomerization over Fluorinated-Alkaline Treated Mordenites.* The yields of branched $C_6$ isomers in the hydroisomerization with microporous MOR/12 without postsynthesis treatment were very low at temperatures ≤200 °C. The yields were increased considerably over the mm-F-MOR/9.4 sample, e.g. from 13.5% to 47.2% at 200 °C, showing that the desilication of fluorinated mordenite zeolite markedly increased the catalytic activity (Figure 8E). This was accompanied by higher yields of dibranched isomers (Table 3) and high selectivity without the detectable formation of $C_1$−$C_4$ byproducts at ≤200 °C (Figure 8F). In comparison with other micromesoporous Pt/H-MOR, the mm-F-MOR/9.4 sample provides the greatest enhancement in the yields of branched $C_6$ isomers achieved at low temperatures (Figure 10).

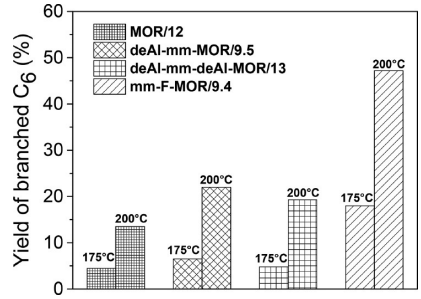


**Figure 10.** Comparison of the effects of the postsynthesis alkaline−acid (Pt/H-deAl-mm-MOR/9.5), acid−alkaline−acid (Pt/H-deAl-mm-deAl-MOR/13), and fluorination−alkaline (Pt/H-mm-F-MOR/9.4) treatments on the yields of branched hexanes at 175 and 200 °C.

The chemical analysis showed the absence of fluorine in the mm-F-MOR/9.4 treated after fluorination by desilication, triple ion exchange with a large excess of $NH_4NO_3$ solution, and calcination in air and subsequently under a hydrogen atmosphere. The enhancement in the activity is thus associated with the micromesoporous structure providing a high concentration of Brønsted sites ($c_B$ = 0.6 mmol $g^{-1}$) readily accessible for *n*-hexane molecules (>90%) (Table 2). To exclude the possible effect of traces of fluoride not detectable by the chemical analysis on the increase in activity, a fluorinated sample of Pt/H-F-ZSM-5 zeolite with small crystals was prepared and its activity was compared with that of Pt/H-ZSM-5. The intracrystalline diffusion does not affect the overall reaction rates for ZSM-5 for either the *n*-hexane hydroisomerization[61] or cracking.[70] Accordingly, we observed very comparable yields of branched $C_6$ isomers over Pt/H-ZSM-5 and its fluorinated analogue Pt/H-F-ZSM-5 in the entire temperature region (Figure S9 in the Supporting Information). Thus, the high concentration of the Brønsted sites located in nonrestricted micropores highly accessible via new channel openings in small mesopores formed by the simultaneous removal of Si and Al atoms results in significantly improved catalytic properties, enabling the reaction at lower temperatures.

## 4. DISCUSSION

**4.1. Structure of Micromesoporous Mordenites Obtained by Leaching Methods.** Selective dissolution of silicon-rich areas of the framework and the extraction of aluminum are inherent parts of the acid and alkali treatments of zeolites, respectively. Our results clearly show that, for the formation of micromesoporous mordenite with Brønsted active sites readily accessible in nonrestricted micropores, it is necessary to extract both silicon and aluminum atoms in a controlled way to ensure the formation of mesopores and preservation of micropores and the majority of the framework Al. Particularly for desilication of mordenites with a high



DOI: 10.1021/acscatal.7b01696
ACS Catal. 2017, 7, 5781−5795

concentration of aluminum in the framework (Si/Al ≈ 12), the extraframework tetrahedrally coordinated $AlO_x/(OH)_y$ species, formed by hydrolysis and dislodgment of a small fraction of framework Al, block a significant part of the pseudomonodimensional 12-ring channels and/or accessibility of the acid sites in 8-ring side pockets. Desilication of mordenite surprisingly does not lead to greater accessibility of the acid sites; to the contrary, a significant part of the micropores is diffusion-limited even for nitrogen molecules. However, subsequent acid leaching under specific conditions, characterized by a low concentration of oxalic or nitric acid, leads to efficient removal of the extraframework and/or perturbed framework Al species formed in mesopores after desilication and blocking of part of the micropores. The concentration of the Brønsted sites determined by $d_3$-acetonitrile and their accessibility for *n*-hexane as a relevant molecular probe for the hydroisomerization reaction indicate that the prevailing amount of the framework Al atoms is not dislodged during either the dissolution of silicon-rich areas of the framework or the selective extraction of the extraframework Al. Thus, the alkaline removal of parts of the Si-rich framework and subsequent selective acid leaching of extraframework Al and only a small amount of framework Al resulted in a micromesoporous mordenite structure with a high concentration of strongly acidic Brønsted sites readily accessible in both 12-ring and 8-ring channels. The desilication with subsequent removal of only extraframework Al creates a number of new channel openings in mesopores, effectively shortening the main 12-ring channels. However, the dealumination of a small fraction of the framework Al atoms is indispensable for significant enhancement of the accessibility of the OH groups in 8-ring side pockets. It should be also mentioned that the increase in the concentration of Lewis centers and an intense signal of internal Si−OH groups suggest that the massive changes in the texture of the zeolite toward a well-developed mesoporous structure leads to the disruption of part of the regularly arranged atoms originally present in the low-defective zeolitic structure.

The alkaline leaching of mordenite preimpregnated with a solution of $NH_4F$ appeared to be the most efficient approach for creating the secondary mesoporous structure in mordenite zeolite with a high concentration of readily accessible Brønsted sites. This procedure enabled controlled extraction of Si atoms and concomitantly the framework F-bearing tetrahedral Al species. The dissolution of tetrahedrally coordinated $Al(FO_3)$ and $SiO_4$ entities during alkaline treatment resulted in secondary mesoporosity and opened nonrestricted channel openings of the preserved microporous structure with a high concentration of Brønsted sites readily accessible for *n*-hexane. A difference was observed in the modes of formation and types of mesoporous structures obtained by desilication−acid treatment and desilication of fluorinated mordenite. With the desilication−acid treatment, circular mesopores 5−20 nm in size were predominant, while desilication of fluorinated mordenite yielded small mesopores combined with mesopores formed along crystal boundaries and intergrowths.

**4.2. Effect of Micromesoporous Structure on Hydroisomerization of *n*-Hexane.** The molecules involved in hydroisomerization as either reactants or products have sizes similar to those of the mordenite pores (Figure 1).[14] Consequently, the access of these molecules to active sites is a key factor governing the performance of mordenite catalysts. The most obvious effects of the introduction of secondary mesoporosity on the yields of branched hexanes obtained in this study is illustrated in Figure 10. Whereas only a small increase in the yield of branched isomers from 13.5% to 16% was obtained after dealumination, the increase in the yield to 22% was appreciable with concurrent introduction of a mesoporous structure by desilication and partial dealumination; note that, at a temperature of 200 °C, the reaction exhibits >99% selectivity for branched isomers and the formation of $C_1-C_5$ byproducts practically did not proceed over any of the analyzed catalysts (Figure 8). The sole partial dealumination significantly improved the accessibility of the OH groups (∼90%) in the mordenite channels, but the benefit was to a significant extent offset by a significant decrease in their concentration. The introduction of a mesoporous structure via subsequent desilication by alkaline treatment and partial dealumination by diluted acid can yield a similar percentage of accessible OH groups to dealumination, but with slightly higher concentrations. Desilication alone yielded mesopores 5−20 nm in size and did not lead to significant exposure of the OH groups to the reactant molecules, and subsequent partial dealumination is also a necessary step in obtaining highly accessible OH groups. This necessarily leads to a reduction in the concentration of OH groups and limits their maximum available concentration. The high accessibility of acid sites in micromesoporous mordenite obtained by sequential alkaline and mild acid treatments is connected with catalytic performance exceeding that of microporous mordenite; however, the improvements in the yields are slight. To attain more significant improvement in the activities, a mordenite structure characterized by a higher concentration of Brønsted sites readily accessible for $C_6$ molecules is crucial. A micromesoporous structure characterized by small mesopores and a high concentration of readily accessible acid sites was obtained by desilication of fluorinated mordenite zeolite. This treatment results in markedly improved catalyst activity and a large increase in the yield of branched isomers (Figures 8 and 10). Thus, it is clear that the micromesoporous structure with a high density of readily accessible OH groups is ultimately connected with catalytic properties greatly exceeding those of microporous or partially dealuminated mordenite zeolite. The concentrations of accessible Brønsted sites were correlated with the activity measured for all of the micromesoporous Pt/H-MOR zeolites (Figure 11). The yields of branched $C_6$ isomers clearly increase with the concentrations of the Brønsted sites accessible for *n*-hexane molecules. We also analyzed the relationships between

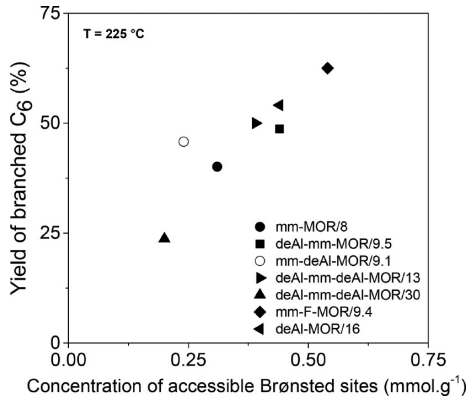


**Figure 11.** Yields of branched $C_6$ isomers in the hydroisomerization of *n*-hexane for Pt/H-MOR zeolites with different concentrations of the accessible Brønsted sites.



DOI: 10.1021/acscatal.7b01696
ACS Catal. 2017, 7, 5781−5795

the concentrations of the Brønsted sites in 8-rings or 12-rings estimated using analysis of the FTIR absorption bands of the bridging OH groups in zeolites (Figure S5 in the Supporting Information) and the hydroisomerization activity (Figure S10 in the Supporting Information). The plots of the yields of branched $C_6$ isomers against the concentrations of the Brønsted sites in 8-ring or 12-ring channels did not show any direct relationship. According to Chiang et al.,[8] the higher activity of the protonic sites in the 8-ring pockets of H-MOR is associated with a specific deformation and partial confinement of the $C_6$ molecule in the 8-ring. In the case of MOR zeolites with hierarchical porosity, the local structure and mainly the openings of the 8-ring pockets are largely affected (see Figure 6) and the specific activity of corresponding protonic sites could be altered.

Summing up, the analysis of the hydroisomerization over micromesoporous Pt/H-MOR zeolites exhibiting quite different levels of hierarchical structure and the overall concentrations of acid sites, and thus the different concentrations of accessible Brønsted sites, shows that the hierarchical porosity has a promotional effect on the activity of acid sites even for the relatively small $C_6$ molecules. The increase in the yields of branched isomers over the micromesoporous structure with a high concentration of readily accessible Brønsted sites enables a shift of the operation window to lower temperatures with more favorable thermodynamic equilibrium for branched isomers.

## CONCLUSIONS

The critical function of the micromesoporous structure and the concentration and accessibility of Brønsted sites for hydroisomerization of linear hexane was elucidated by using three series of micromesoporous mordenite zeolites differing in their mesoporosity and concentration and the accessibility of acid sites. The hydroisomerization of *n*-hexane over microporous Pt/H-mordenite is limited by mass transfer effects due to the low accessibility of acid sites in 8-ring channels and the diffusion-restricted pseudomonodimensional channel structure. The introduction of secondary mesoporosity into mordenite using the alkaline−acid, acid−alkaline−acid, and fluorination−alkaline postsynthesis treatments proposed in this study effectively shortens the length of the 12-ring main channels, opens the side 8-ring channel pockets, provides a high concentration of Brønsted sites, and enhances the accessibility of the acid sites for hexane molecules. The shortening of the main 12-ring channels and a larger number of channel openings provide an increase in the selectivity, limiting the nonselective subsequent cracking reactions and consequently increasing the yield of the desired products at higher temperatures. The micromesoporous mordenite structure with the Brønsted sites in the environment of the micropores and accessible through mesopores alleviates the diffusion limitations due to restricted access and slow transport to/from the active site, resulting in a significant increase in the catalyst efficiency and improvements in the selectivity in skeletal hydroisomerization of *n*-hexane into branched isomers. It enables efficient isomerization in a temperature region that is thermodynamically more favorable for desired dibranched isomers.

## ASSOCIATED CONTENT

### Supporting Information

The Supporting Information is available free of charge on the ACS Publications website at DOI: 10.1021/acscatal.7b01696.

Description of the structure of parent mordenite zeolite, SEM images, X-ray diffraction patterns, nitrogen adsorption and desorption on a log *P* scale, and $^{27}$Al MAS NMR spectra for the micromesoporous mordenite zeolites, illustration of analysis of the FTIR absorption bands of the bridging OH groups of dehydrated zeolites and the C≡N groups of adsorbed $d_3$-acetonitrile, illustration of analysis of the OH group accessibility using FTIR spectra of adsorbed *n*-hexane, TEM images and FTIR spectra of CO adsorbed on the reduced microporous and micromesoporous Pt/H-MOR, and supplementary kinetic data (PDF)

## AUTHOR INFORMATION


### Corresponding Author

*E-mail for P.S.: petr.sazama@jh-inst.cas.cz.

### ORCID

Petr Sazama: 0000-0001-7795-2681


### Notes

The authors declare no competing financial interest.

## ACKNOWLEDGMENTS

This work was supported by the Grant Agency of the Czech Republic under Project No. GA15-12113S. The authors acknowledge the assistance provided by the Research Infrastructures NanoEnviCz (Project No. LM2015073) and Pro-NanoEnviCz (Project No. CZ.02.1.01/0.0/0.0/16_013/0001821), supported by the Ministry of Education, Youth and Sports of the Czech Republic.

## REFERENCES


(1) Iglesia, E.; Soled, S. L.; Kramer, G. M. *J. Catal.* **1993**, *144*, 238−253.
(2) Iglesia, E.; Barton, D. G.; Soled, S. L.; Miseo, S.; Baumgartner, J. E.; Gates, W. E.; Fuentes, G. A.; Meitzner, G. D. Selective isomerization of alkanes on supported tungsten oxide acids. *Stud. Surf. Sci. Catal.* **1996**, *101*, 533−542.
(3) Chica, A.; Corma, A. *J. Catal.* **1999**, *187*, 167−176.
(4) Ono, Y. *Catal. Today* **2003**, *81*, 3−16.
(5) Tromp, M.; van Bokhoven, J. A.; Garriga Oostenbrink, M. T.; Bitter, J. H.; de Jong, K. P.; Koningsberger, D. C. *J. Catal.* **2000**, *190*, 209−214.
(6) Gounder, R.; Iglesia, E. *Angew. Chem., Int. Ed.* **2010**, *49*, 808−811.
(7) Bhan, A.; Iglesia, E. *Acc. Chem. Res.* **2008**, *41*, 559−567.
(8) Chiang, H.; Bhan, A. *J. Catal.* **2011**, *283*, 98−107.
(9) Van Laak, A. N. C.; Sagala, S. L.; Zecevic, J.; Friedrich, H.; De Jongh, P. E.; De Jong, K. P. *J. Catal.* **2010**, *276*, 170−180.
(10) Centi, G.; Perathoner, S. *Coord. Chem. Rev.* **2011**, *255*, 1480−1498.
(11) Groen, J. C.; Zhu, W.; Brouwer, S.; Huynink, S. J.; Kapteijn, F.; Moulijn, J. A.; Pérez-Ramírez, J. *J. Am. Chem. Soc.* **2007**, *129*, 355−360.
(12) Gobin, O. C.; Reitmeier, S. J.; Jentys, A.; Lercher, J. A. *J. Phys. Chem. C* **2011**, *115*, 1171−1179.
(13) Park, D. H.; Kim, S. S.; Wang, H.; Pinnavaia, T. J.; Papapetrou, M. C.; Lappas, A. A.; Triantafyllidis, K. S. *Angew. Chem., Int. Ed.* **2009**, *48*, 7645−7648.
(14) Ferreira, A. F. P.; Mittelmeijer-Hazeleger, M. C.; Granato, M. A.; Martins, V. F. D.; Rodrigues, A. E.; Rothenberg, G. *Phys. Chem. Chem. Phys.* **2013**, *15*, 8795−8804.
(15) Fan, W.; Snyder, M. A.; Kumar, S.; Lee, P. S.; Yoo, W. C.; McCormick, A. V.; Lee Penn, R.; Stein, A.; Tsapatsis, M. *Nat. Mater.* **2008**, *7*, 984−991.
(16) Hartmann, M. *Angew. Chem., Int. Ed.* **2004**, *43*, 5880−5882.
(17) Inayat, A.; Knoke, I.; Spiecker, E.; Schwieger, W. *Angew. Chem., Int. Ed.* **2012**, *51*, 1962−1965.




DOI: 10.1021/acscatal.7b01696
*ACS Catal.* 2017, 7, 5781−5795

(18) Perez-Ramirez, J. *Nat. Chem.* **2012**, *4*, 250−251.
(19) Sazama, P.; Sobalik, Z.; Dedecek, J.; Jakubec, I.; Parvulescu, V.; Bastl, Z.; Rathousky, J.; Jirglova, H. *Angew. Chem., Int. Ed.* **2013**, *52*, 2038−2041.
(20) Sun, J. L.; Bonneau, C.; Cantin, A.; Corma, A.; Diaz-Cabanas, M. J.; Moliner, M.; Zhang, D. L.; Li, M. R.; Zou, X. D. *Nature* **2009**, *458*, 1154−1157.
(21) Choi, M.; Na, K.; Kim, J.; Sakamoto, Y.; Terasaki, O.; Ryoo, R. *Nature* **2009**, *461*, 246−249.
(22) Zhang, X. Y.; Liu, D. X.; Xu, D. D.; Asahina, S.; Cychosz, K. A.; Agrawal, K. V.; Al Wahedi, Y.; Bhan, A.; Al Hashimi, S.; Terasaki, O.; Thommes, M.; Tsapatsis, M. *Science* **2012**, *336*, 1684−1687.
(23) Jacobsen, C. J. H.; Madsen, C.; Houzvicka, J.; Schmidt, I.; Carlsson, A. *J. Am. Chem. Soc.* **2000**, *122*, 7116−7117.
(24) De Jong, K. P.; Zecevic, J.; Friedrich, H.; De Jongh, P. E.; Bulut, M.; Van Donk, S.; Kenmogne, R.; Finiels, A.; Hulea, V.; Fajula, F. *Angew. Chem., Int. Ed.* **2010**, *49*, 10074−10078.
(25) Groen, J. C.; Moulijn, J. A.; Perez-Ramirez, J. *J. Mater. Chem.* **2006**, *16*, 2121−2131.
(26) Góra-Marek, K.; Tarach, K.; Tekla, J.; Olejniczak, Z.; Kuśtrowski, P.; Liu, L.; Martinez-Triguero, J.; Rey, F. *J. Phys. Chem. C* **2014**, *118*, 28043−28054.
(27) Paixao, V.; Carvalho, A. P.; Rocha, J.; Fernandes, A.; Martins, A. *Microporous Mesoporous Mater.* **2010**, *131*, 350−357.
(28) Wichterlova, B.; Tvaruzkova, Z.; Sobalik, Z.; Sarv, P. *Microporous Mesoporous Mater.* **1998**, *24*, 223−233.
(29) Fyfe, C. A.; Feng, Y.; Grondey, H.; Kokotailo, G. T.; Gies, H. *Chem. Rev. (Washington, DC, U. S.)* **1991**, *91*, 1525−1543.
(30) Engelhardt, G.; Lohse, U.; Lippmaa, E.; Tarmak, M.; Magi, M. *Z. Anorg. Allg. Chem.* **1981**, *482*, 49−64.
(31) Eder, F.; Stockenhuber, M.; Lercher, J. A. *J. Phys. Chem. B* **1997**, *101*, 5414−5419.
(32) Zholobenko, V. L.; Makarova, M. A.; Dwyer, J. *J. Phys. Chem.* **1993**, *97*, 5962−5964.
(33) Bordiga, S.; Lamberti, C.; Geobaldo, F.; Zecchina, A.; Palomino, G. T.; Arean, C. O. *Langmuir* **1995**, *11*, 527−533.
(34) Wakabayashi, F.; Kondo, J.; Wada, A.; Domen, K.; Hirose, C. *J. Phys. Chem.* **1993**, *97*, 10761−10768.
(35) Alberti, A. *Zeolites* **1997**, *19*, 411−415.
(36) Eder, F.; Stockenhuber, M.; Lercher, J. A. *J. Phys. Chem. B* **1997**, *101*, 5414−5419.
(37) Viswanadham, N.; Kumar, M. *Microporous Mesoporous Mater.* **2006**, *92*, 31−37.
(38) Lietz, G.; Schnabel, K. H.; Peuker, C.; Gross, T.; Storek, W.; Volter, J. *J. Catal.* **1994**, *148*, 562−568.
(39) Remy, M. J.; Stanica, D.; Poncelet, G.; Feijen, E. J. P.; Grobet, P. J.; Martens, J. A.; Jacobs, P. A. *J. Phys. Chem.* **1996**, *100*, 12440−12447.
(40) Chen, T. H.; Wouters, B.; Grobet, P. *Chem. J. Internet* **2000**, *2*, 7−13.
(41) Chen, T. H.; Wouters, B. H.; Grobet, P. J. *Eur. J. Inorg. Chem.* **2000**, *2000*, 281−285.
(42) Wouters, B. H.; Chen, T.; Grobet, P. J. *J. Phys. Chem. B* **2001**, *105*, 1135−1139.
(43) Chen, J.; Chen, T.; Guan, N.; Wang, J. *Catal. Today* **2004**, *93*−*95*, 627−630.
(44) Samoson, A.; Lippmaa, E.; Engelhardt, G.; Lohse, U.; Jerschkewitz, H. G. *Chem. Phys. Lett.* **1987**, *134*, 589−592.
(45) Sazama, P.; Wichterlova, B.; Dedecek, J.; Tvaruzkova, Z.; Musilova, Z.; Palumbo, L.; Sklenak, S.; Gonsiorova, O. *Microporous Mesoporous Mater.* **2011**, *143*, 87−96.
(46) Sayed, M. B.; Kydd, R. A.; Cooney, R. P. *J. Catal.* **1984**, *88*, 137−149.
(47) Kustov, L. M.; Kazansky, V. B.; Beran, S.; Kubelkova, L.; Jiru, P. *J. Phys. Chem.* **1987**, *91*, 5247−5251.
(48) Fritz, P. O.; Lunsford, J. H. *J. Catal.* **1989**, *118*, 85−98.
(49) Groen, J. C.; Jansen, J. C.; Moulijn, J. A.; Pérez-Ramírez, J. *J. Phys. Chem. B* **2004**, *108*, 13062−13065.
(50) Svelle, S.; Sommer, L.; Barbera, K.; Vennestrøm, P. N. R.; Olsbye, U.; Lillerud, K. P.; Bordiga, S.; Pan, Y. H.; Beato, P. *Catal. Today* **2011**, *168*, 38−47.
(51) Giudici, R.; Kouwenhoven, H. W.; Prins, R. *Appl. Catal., A* **2000**, *203*, 101−110.
(52) Van Geem, P. C.; Scholle, K. F. M. G. J.; Van Der Velden, G. P. M.; Veeman, W. S. *J. Phys. Chem.* **1988**, *92*, 1585−1589.
(53) Muller, M.; Harvey, G.; Prins, R. *Microporous Mesoporous Mater.* **2000**, *34*, 135−147.
(54) Silaghi, M.-C.; Chizallet, C.; Sauer, J.; Raybaud, P. *J. Catal.* **2016**, *339*, 242−255.
(55) Yu, L.; Huang, S.; Miao, S.; Chen, F.; Zhang, S.; Liu, Z.; Xie, S.; Xu, L. *Chem. - Eur. J.* **2015**, *21*, 1048−1054.
(56) Qin, Z.; Lakiss, L.; Gilson, J. P.; Thomas, K.; Goupil, J. M.; Fernandez, C.; Valtchev, V. *Chem. Mater.* **2013**, *25*, 2759−2766.
(57) Pérez-Ramírez, J.; Christensen, C. H.; Egeblad, K.; Christensen, C. H.; Groen, J. C. *Chem. Soc. Rev.* **2008**, *37*, 2530−2542.
(58) Milina, M.; Mitchell, S.; Crivelli, P.; Cooke, D.; Pérez-Ramírez, J. *Nat. Commun.* **2014**, *5*, 3922.
(59) Reitmeier, S. J.; Gobin, O. C.; Jentys, A.; Lercher, J. A. *Angew. Chem., Int. Ed.* **2009**, *48*, 533−538.
(60) Ribeiro, F.; Marcilly, C.; Guisnet, M. *J. Catal.* **1982**, *78*, 267−274.
(61) Van De Runstraat, A.; Kamp, J. A.; Stobbelaar, P. J.; Van Grondelle, J.; Krijnen, S.; Van Santen, R. A. *J. Catal.* **1997**, *171*, 77−84.
(62) Stakheev, A. Y.; Shpiro, E. S.; Tkachenko, O. P.; Jaeger, N. I.; Schulz-Ekloff, G. *J. Catal.* **1997**, *169*, 382−388.
(63) Kubanek, P.; Schmidt, H. W.; Spliethoff, B.; Schüth, F. *Microporous Mesoporous Mater.* **2005**, *77*, 89−96.
(64) Monteiro, R.; Ania, C. O.; Rocha, J.; Carvalho, A. P.; Martins, A. *Appl. Catal., A* **2014**, *476*, 148−157.
(65) Zecevic, J.; Vanbutsele, G.; De Jong, K. P.; Martens, J. A. *Nature* **2015**, *528*, 245−254.
(66) Sazama, P.; Kaucky, D.; Moravkova, J.; Pilar, R.; Klein, P.; Pastvova, J.; Tabor, E.; Sklenak, S.; Jakubec, I.; Mokrzycki, L. *Appl. Catal., A* **2017**, *533*, 28−37.
(67) Monteiro, R.; Ania, C. O.; Rocha, J.; Carvalho, A. P.; Martins, A. *Appl. Catal., A* **2014**, *476*, 148−157.
(68) Leng, K.; Wang, Y.; Hou, C.; Lancelot, C.; Lamonier, C.; Rives, A.; Sun, Y. *J. Catal.* **2013**, *306*, 100−108.
(69) Nesterenko, N. S.; Thibault-Starzyk, F.; Montouillout, V.; Yuschenko, V. V.; Fernandez, C.; Gilson, J. P.; Fajula, F.; Ivanova, I. I. *Microporous Mesoporous Mater.* **2004**, *71*, 157−166.
(70) Haag, W. O.; Lago, R. M.; Weisz, P. B. *Faraday Discuss. Chem. Soc.* **1981**, *72*, 317−330.


DOI: 10.1021/acscatal.7b01696
*ACS Catal.* 2017, 7, 5781−5795